Ceramics International 46 (2020) 8601–8614

Contents lists available at ScienceDirect

Ceramics International

journal homepage: www.elsevier.com/locate/ceramint

Physicochemical and thermo physical characterization of $CaO–CaF_2–SiO_2$ and $CaO–TiO_2–SiO_2$ based electrode coating for offshore welds

Waris Nawaz Khan*, Rahul Chhibber

Department of Mechanical Engineering, Indian Institute of Technology Jodhpur, India

ARTICLE INFO

Keywords:
Physicochemical properties
Thermo-physical properties
Welding
Offshore structures
Powder
Optimization

ABSTRACT

This paper investigates the physicochemical and thermo-physical properties of $CaO–CaF_2–SiO_2$ and $CaO–TiO_2–SiO_2$ based electrode coating for welding offshore structures. Twenty-one electrode coating compositions have been formulated using extreme vertices design method. The coating was crushed to powder form. The powder was characterized for weight loss, density, specific heat, enthalpy, thermal conductivity, diffusivity, and specific heat. Coating's structural analysis was done using X-Ray Diffraction and Fourier transformation. X-Ray Fluorescence, Thermogravimetric Analyzer, and Hot disc have been used to characterize the coating mixture. The regression analysis has been used to study the effect of individual constituents and their binary, tertiary interactions on the properties. The obtained output of properties has been optimized using multi-response optimization.

1. Introduction

The past decade has seen a considerable increase in the total share of oil and gas production from offshore sites. This is expected to further increase in the future. Offshore drilling and transportation of natural gas, hydrocarbon, and oil become very challenging because of severe working conditions, which include high temperature and pressure, corrosive environment with high $H_2S–CO_2$ level. The welds at offshore sites are expected to have high structural integrity and perform well in aggressive conditions [1,2]. Super duplex stainless steel due to its enhanced corrosion resistance and excellent mechanical properties is one of the most preferred materials for offshore application. It is widely used for applications such as hydrocarbon drilling risers, gas transmission lines, pressure vessels, storage vessels, and heat exchangers [3,4]. Maintaining the structural integrity of dissimilar welds is more challenging because of issues such as mechanical mismatch, carbon migration, metallurgical deterioration, residual stress development. [5–7] Weld properties depend mainly upon the filler wire and coating constituents. In the Shielded Metal Arc Welding (SMAW) process, the coated electrodes protect the weld metal from surrounding impurities, act as arc stabilizers and deoxidizer. It also influences weld chemistry by controlling element transfer [8]. The constituents of coating are transferred to the weld pool and from molten pool to slag through gas-metal and slag metal reactions, respectively. The behavior of coatings mixture depends mainly on its physicochemical and thermophysical properties. A highly viscous electrode coating decreases the fluidity of the molten pool; similarly, one with high negative enthalpy is expected to affect the weld region, and heat-affected zone and thermo mechanical affected zone adversely. Previous researchers have studied the effect of flux constituents on the mechanical performance of weld and its chemistry [9–12]. Limited literature is available on the physicochemical and thermophysical characterization of flux and coating [13–15].This paper investigates the physicochemical and thermo physical properties of electrode coating developed for offshore welds using $CaO–CaF_2–SiO_2$ and $CaO–TiO_2–SiO_2$ system. The coating mixture in powder form has been characterized for density, thermal conductivity, weight loss upon heating, thermal diffusivity, specific heat, and enthalpy change. Various characterization techniques have been used, which includes hot disc, thermogravimetric analyzer. Structural analysis of coating has been done using X-Ray Diffraction (XRD), and Fourier Transformation (FTIR). The regression model for each response was developed, and the effect of individual constituents and their binary, tertiary interaction on output was analyzed. The developed model has also been validated by comparing the difference between actual and predicted values. Multi response optimization has been carried out to obtain the optimum flux composition, which satisfies the desired target range for all response values.

* Corresponding author.
E-mail addresses: khan.3@iitj.ac.in (W.N. Khan), rahul_chhibber@iitj.ac.in (R. Chhibber).

https://doi.org/10.1016/j.ceramint.2019.12.092
Received 26 August 2019; Received in revised form 29 November 2019; Accepted 9 December 2019
Available online 16 December 2019

Table 1
Chemical composition of minerals (wt. %).

S. No	Mineral Powder	Source Of	Chemical Composition (wt.%)						
			Al	Si	Ca	Ti	Fe	Mg	S
1	Calcite	CaO	4.61	2.95	81.45	–	0.74	9.48	–
2	Fluorspar	CaF_2	4.97	1.38	92.77	–	0.41	–	–
3	Silica	SiO_2	2.82	96.16	0.48	–	0.17	–	0.29
4	Rutile	TiO_2	5.94	4.09	–	87.46	1.57	–	0.29

Table 2
Chemical composition of red ochre (wt. %).

Specimen	Fe_2O_3	SiO_2	Al_2O_3	H_2O
Red Ochre	59.875	7.12	2.6	0.55

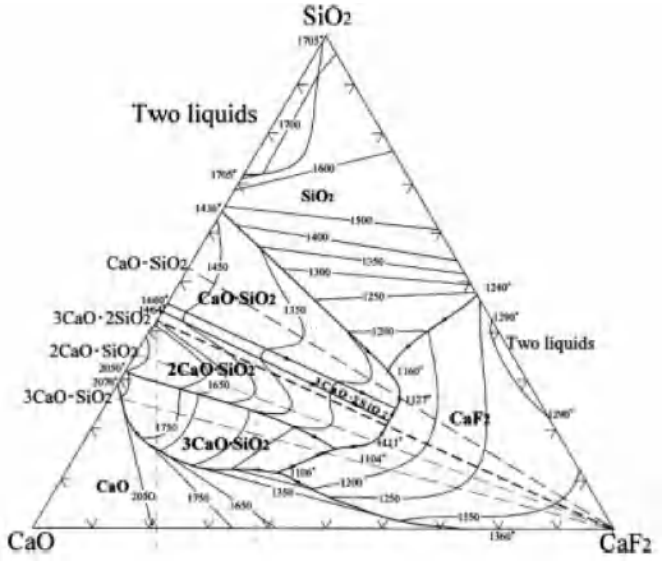

Fig. 1. Ternary Phase Diagram of SiO_2–CaO–CaF_2 system [25].

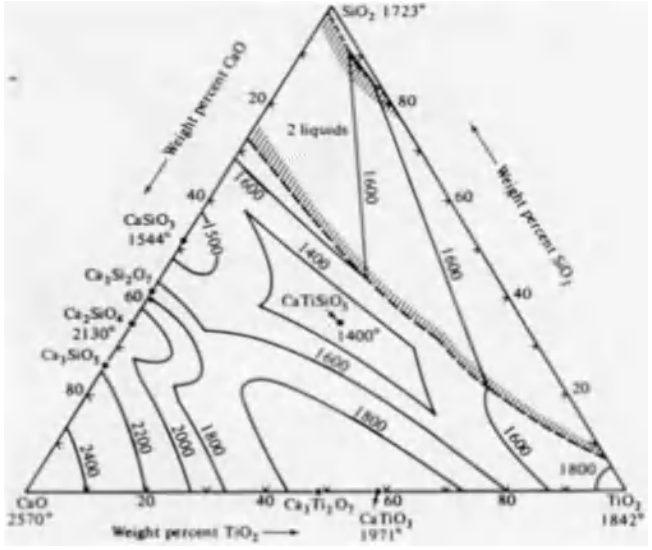

Fig. 2. Ternary Phase Diagram of SiO_2–CaO–TiO_2 system [26].

Table 3
Design Matrix for 21 flux compositions.

Coating Number	Flux	Basicity Index	Nature of Point	Composition of Mixture			
				CaO	CaF_2	TiO_2	SiO_2
1	F1	2.44	V	30.00	25.00	25.00	10.00
2	F2	2.44	V	35.00	20.00	25.00	10.00
3	F3	3.00	V	35.00	25.00	20.00	10.00
4	F4	3.06	V	32.50	25.00	27.50	5.00
5	F5	2.66	V	31.50	21.25	30.00	7.50
6	F6	2.00	V	25.00	25.00	30.00	10.00
7	F7	2.58	EC	32.50	22.50	27.50	7.50
8	F8	2.33	EC	35.00	17.50	30.00	7.50
9	F9	3.42	EC	35.00	25.00	25.00	5.00
10	F10	2.72	EC	35.00	21.25	26.25	7.50
11	F11	2.95	EC	33.33	23.33	28.33	5.00
12	F12	2.75	EC	30.00	25.00	30.00	5.00
13	F13	2.28	EC	31.66	21.66	26.66	10.00
14	F14	2.72	EC	31.25	25.00	26.25	7.50
15	F15	2.75	EC	35.00	20.00	30.00	5.00
16	F16	2.00	PC	35.00	15.00	30.00	10.00
17	F17	2.75	PC	32.50	22.50	30.00	5.00
18	F18	2.00	PC	30.00	20.00	30.00	10.00
19	F19	3.06	PC	35.00	22.50	27.50	5.00
20	F20	2.33	PC	27.50	25.00	30.00	7.50
21	F21	3.20	OC	35.00	25.00	22.5	7.50

V: Vertex, EC: Edge Centre, PC: Plane Centre, OC: Overall Centroid.

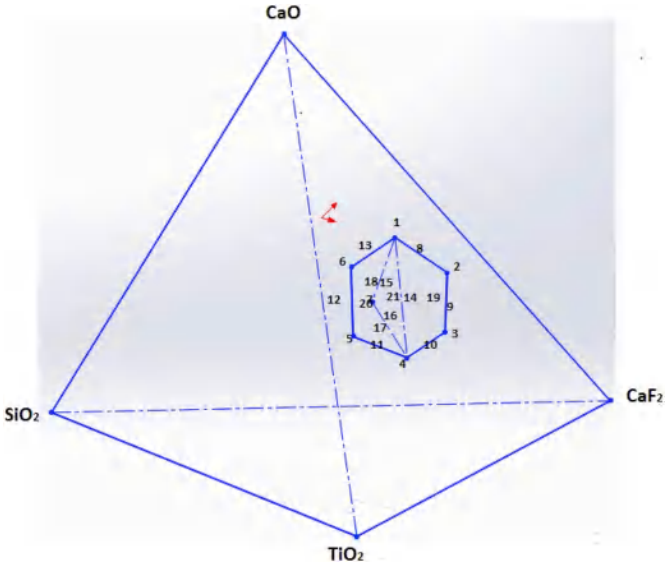

Fig. 3. Design space diagram.

2. Materials

The electrode coating was prepared based on the varying composition of four different minerals, namely Calcite, Fluorspar, Rutile, and Silica. High basicity index electrodes were developed as it is desirable for marine and offshore application. X-Ray Fluorescence of mineral constituents was done, and results are summarized in Table 1.

Mineral waste red ochre was added to the coating composition. Red ochre is a waste from an iron ore mining site, which is anhydrous iron oxide. It takes a red color from a haematite mineral. Ferrous ion and iron-oxidizing bacteria are the primary raw material behind the red

Table 4
Thermal characterization of coating.

Coating	Thermal Conductivity (W/mK)	Thermal Diffusivity (mm^2/s)	Specific Heat (MJ/m^3K)
1	0.3209	0.2642	1.214
2	0.3341	0.3328	1.004
3	0.3026	0.2699	1.121
4	0.3105	0.3756	0.8267
5	0.3118	0.3111	1.002
6	0.2682	0.2526	1.062
7	0.3094	0.3232	0.9572
8	0.2660	0.2720	0.9781
9	0.2677	0.2604	1.028
10	0.2488	0.3011	0.8264
11	0.2783	0.2816	0.9883
12	0.2493	0.2540	0.9815
13	0.2448	0.2349	1.042
14	0.2640	0.2379	1.109
15	0.2339	0.2175	1.076
16	0.2583	0.2625	0.9840
17	0.2458	0.2443	1.006
18	0.2679	0.2506	1.069
19	0.2360	0.2216	1.065
20	0.2701	0.2314	1.167
21	0.2717	0.2618	1.038

Table 5
Density Measurement of coating specimen.

Coating	Weight of coating (g)	Volume (cm^3)	Density (g/cm^3)
1	14.71	10	1.471
2	14.27	10	1.427
3	14.02	10	1.402
4	14.67	10	1.467
5	14.88	10	1.488
6	14.78	10	1.478
7	14.32	10	1.432
8	14.02	10	1.402
9	14.08	10	1.408
10	13.90	10	1.390
11	14.00	10	1.400
12	14.20	10	1.420
13	14.4	10	1.440
14	13.8	10	1.380
15	14.3	10	1.430
16	14.4	10	1.440
17	13.6	10	1.360
18	13.9	10	1.390
19	13.6	10	1.360
20	13.9	10	1.390
21	14.2	10	1.420

ochre formation. When the iron-rich rocks from the mining site enter the drain tile, the bacteria oxidize the ferrous ions. This combined oxidized product of iron along with bacterial slime constitutes iron ochre. The sample of red ochre used in this experiment was collected from an iron ore situated in the Rajasthan state of India. Table 2 represents the chemical composition of red ochre waste. The main reason behind adding red ochre was to utilize the property of iron to improve arc stability and current carrying capacity. Available literature reveals that most of the reported research has been focused upon utilization of red mud, a mineral waste from bauxite ore, whereas other wastes still remain unexplored. Moreover, the scope of utilizing mineral wastes in welding consumables hasn't been opened much [16–22].

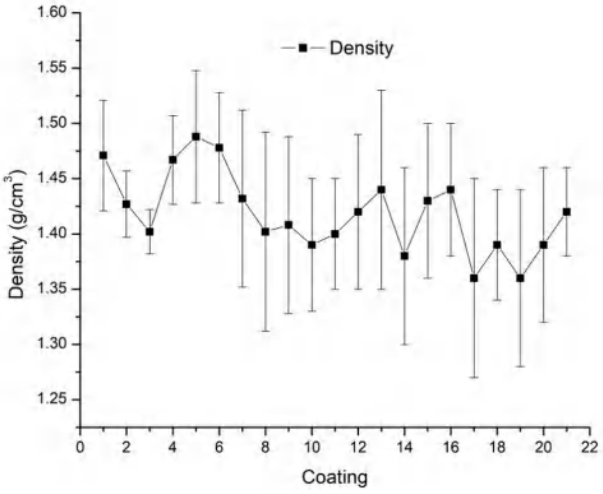

Fig. 4. Density of coating mixture.

Table 6
Weight loss in thermogravimetric analysis.

Coating	Initial Weight (W_i)	Final Weight (W_f)	Change in Weight ($\Delta W = W_i - W_f$)	Change in Weight (%ΔW)
1	14.774	12.608	2.166	14.66
2	21.603	18.316	3.287	15.21
3	10.732	8.998	1.734	16.15
4	13.674	11.293	2.381	17.41
5	11.691	9.867	1.824	15.60
6	11.871	10.334	1.537	12.94
7	13.524	11.828	1.696	12.54
8	11.087	9.04	2.047	18.46
9	14.133	11.673	2.46	17.40
10	11.593	9.461	2.132	18.39
11	14.623	12.493	2.13	14.56
12	12.845	10.862	1.983	15.43
13	11.08	9.0219	2.058	18.57
14	13.672	11.643	2.029	14.84
15	12.103	9.958	2.145	17.72
16	16.503	13.83	2.673	16.19
17	17.894	15.108	2.786	15.56
18	18.517	15.883	2.634	14.22
19	15.545	13.5	2.045	13.16
20	13.878	11.858	2.02	14.56
21	12.946	10.963	1.983	15.32

3. Design of experiment

The electrode coating formulation was designed using extreme vertices design as suggested by McLean and Anderson [23]. The constrained mixture design for a mixture of n components between the upper and lower limits is expressed mathematically as: [24]

$$0 \le \alpha_i \le x_i \le \beta_i \le 100 \quad (1)$$

and

$$\sum_{i=1}^{n} x_i \quad (2)$$

Where i = 1, 2, 3, ..., n; α_i and β_i are the upper and lower constraints on the x_i, which is the percentage composition of individual constituents. In the SMAW process, the coating should melt before the melting of base metal and should remain in the molten state even after

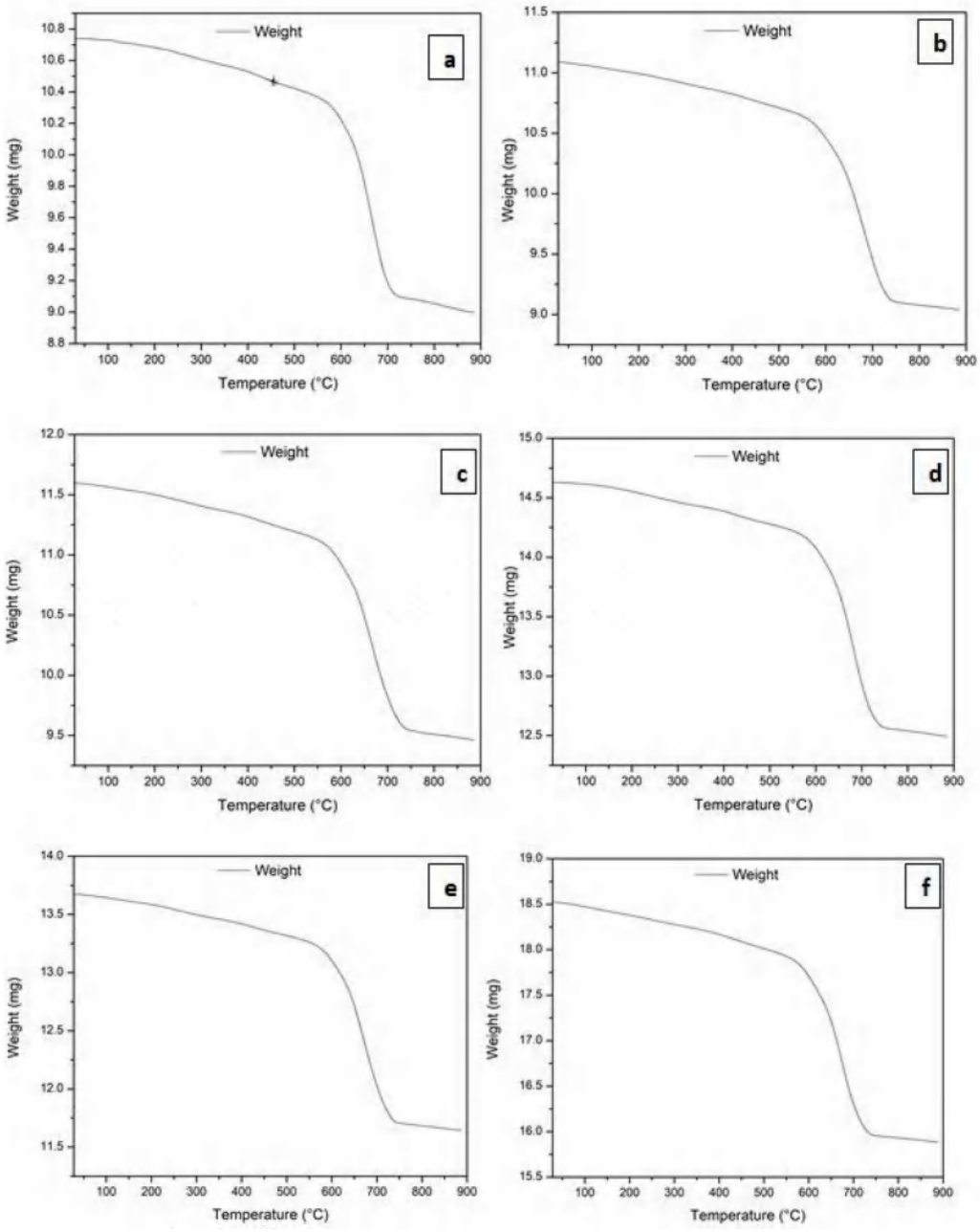

Fig. 5. Weight Loss occurring in coating: (a) Coating 3 (b) Coating 8 (c) Coating 10 (d) Coating 11 (e) Coating 14 (f) Coating 18.

the solidification of the weld. This fact has been kept into consideration while deciding the composition mixture so that the composite melting temperature of the coating mixture remains well under the limit. The ternary phase diagram of SiO_2–CaO–CaF_2 and SiO_2–CaO–TiO_2 system (Fig. 1 and Fig. 2) has been used to identify the points corresponding to the low melting point and corresponding design space.

The upper and lower limit of the four mineral constituents was estimated using the ternary phase diagram. This estimated upper and lower limit of constituents was scaled down to a total of 90% to accommodate 5% red ochre and other essential commodities in 5% composition by weight. Equation (3) shows the upper and lower limit of percentage composition for each constituent and their total is in Equation (4).

$$25 \leq \mathrm{CaO}\ (x_1) \leq 35 \tag{3}$$

$$15 \leq \mathrm{CaF2}\ (x_2) \leq 25$$

$$20 \leq \mathrm{TiO2}\ (x_3) \leq 30$$

$$5 \leq \mathrm{SiO2}\ (x_4) \leq 10$$

$$\sum_{i=1}^{4} x_i = 90 \tag{4}$$

Table 3 represents the design matrix for 21 flux composition

Table 7
Enthalpy measurement of coating specimens.

Coating	Peak Temperature (^{0}C)	Enthalpy (ΔH in J/g)
1	402.85	−18483.1289
2	364.88	−11770.0279
3	394.52	−26157.3258
4	369.36	−18777.9303
5	362.01	−19424.3895
6	376.49	−22848.6118
7	387.57	−19845.2530
8	371.53	−24956.2674
9	347.85	−14819.1628
10	378.87	−21460.1018
11	406.35	−18593.4182
12	377.26	−20711.5693
13	364.09	−22155.1363
14	373.54	−17315.1390
15	359.64	−17811.3754
16	349.90	−13095.3414
17	356.37	−12871.5955
18	347.51	−13693.7854
19	350.02	−13482.5273
20	389.63	−17127.4561
21	364.25	−17672.2341

formulation. The three-dimensional space diagram for the mixture is shown in Fig. 3. The space diagram has six vertices, nine-edge centers, five plane centers, and one overall centroid.

4. Experimentation

The constituent mineral powders were individually weighed as per the design matrix along with 5% by weight, red ochre, and mixed properly in the dry mixer. Potassium Silicate, a binder was then added, and the wet mixture was prepared. The composition was left to get mixed for 45 min in the mixer. The mixture was then extruded on to the filler wire of 309 L austenitic stainless steel using a lab-scale extruder. The electrodes were then air-dried for 48 h and then baked in an oven at a temperature of 360 °C for 90 min. After this, the electrode coating was removed from the filler wire and crushed to a size of approximately 240 μm. These were then subjected to several characterizations. Bulk density measurement was done by weighing the amount of coating powder, which occupies 10 mL volume in a measuring cylinder. This ratio of mass in grams to the volume occupied in cm^3 gives the measure of coating density. Structural analysis of coating specimens was carried out with the X-Ray diffraction technique using mono chromated Cu Kα radiation. Fourier Transformed Infrared Spectrometer (FTIR) method with a resolution of 2 cm^{-1} in the wavenumber range of 400–4000 cm^{-1} was done to analyze the different bonds and bond lengths present in the mixture. Enthalpy and weight loss were calculated by heating the sample from 30 °C to 900 °C at a constant rate of 20 °C/min. This analysis was carried out in the Thermogravimetric Analyzer. Hot disc technique was employed to measure the thermal behavior of electrode coating in terms of thermal conductivity, diffusivity, and specific heat. The measurement was done using Kapton sensor of 3.415 mm size.

5. Results

Thermal characterization results of coating samples performed on the hot disc are summarized in Table 4. Coating 2 has the maximum thermal conductivity of 0.3341 W/mK, whereas coating mixture 4 has maximum thermal diffusivity of 0.3756 mm^2/s. Specific heat has a maximum value of 1.214 MJ/m^3K for coating 1. The thermal conductivity is calculated on the principle of Fourier's equation, which is expressed mathematically as in Equation (5).

$$K = \frac{QL}{AdT}. \tag{5}$$

Where K is thermal conductivity in W/mK, Q is the amount of heat transferring through material measured in W. Area of the contact surface is represented by A in m^2, dT is the difference in temperature measured in Kelvin. Thermal diffusivity is the measure of how fast a material can absorb heat from its surrounding. Mathematically it is calculated using Equation (6).

$$\alpha = \frac{K}{\rho Cp} \tag{6}$$

Where K is thermal conductivity in W/mK, ρ is density in kg/m^3, and Cp is specific heat capacity in J/kg K. Specific heat is defined as the amount of heat required to raise the temperature of the specimen by 1 °C. It is given by Equation (7).

$$s = \frac{Q}{mdT} \tag{7}$$

The bulk density measure of the coating was carried out by putting the coating powder in a measuring cylinder. The amount of crushed coating powder occupying 10 mL volume was weighed on a weighing balance with a resolution of ± 0.01 g. The observed weight of crushed coating and corresponding density measurement is reported in Table 3. The bulk density method's mathematical expression is given in Equation (8).

$$\rho = \frac{m}{V} \tag{8}$$

Where ρ is density in g/cm^3, m is the weight of powder measured on weigh balance in grams, and V here is the displaced volume, which is 10 cm^3 for each specimen. Three measurements for each coating specimen were made, and this paper reports the mean density value. Table 5 gives the density measurement for all specimens. Fig. 4 shows the mean density variation across all specimens.

Enthalpy change and weight loss associated with coating compositions were measured in Thermogravimetric Analyzer. Thermogravimetric Analysis measures the change in weight of powder specimen as a function of time and temperature. Here the sample was initially heated from its initial temperature to 30 °C and then given a hold time of 1 min. The specimen was then linearly heated from 30 °C to 900 °C at a constant rate of 20 °C/minute in a controlled atmosphere. Corresponding loss in weight was achieved and is reported in Table 6. Lower the weight loss, more thermally stable the coating mixture is, hence it is always desirable that electrode coating constituents should have low percentage weight loss at high temperature. In the given mixture compositions, the coating composition 7 has the most thermostable behavior with minimum weight loss of 12.54% of its initial weight. Coating 13 has the greatest change in weight percentage of 18.57% and represents a thermally least stable composition. Fig. 5 shows the weight loss occurring owing to heating up to a temperature of 900 °C.

Thermogravimetric Analysis also gives data related to enthalpy associated with the heating of the powder sample. Enthalpy is the thermodynamic property of a system, which represents total heat associated with the process. It is the sum of internal energy along with the product of pressure and volume. It represents how much work was added to the system or was done by the system while undergoing a certain process. A positive enthalpy value represents the work was done on the system, which implies that the head was absorbed during the process. Whereas the negative value of enthalpy means work was done by the system, and

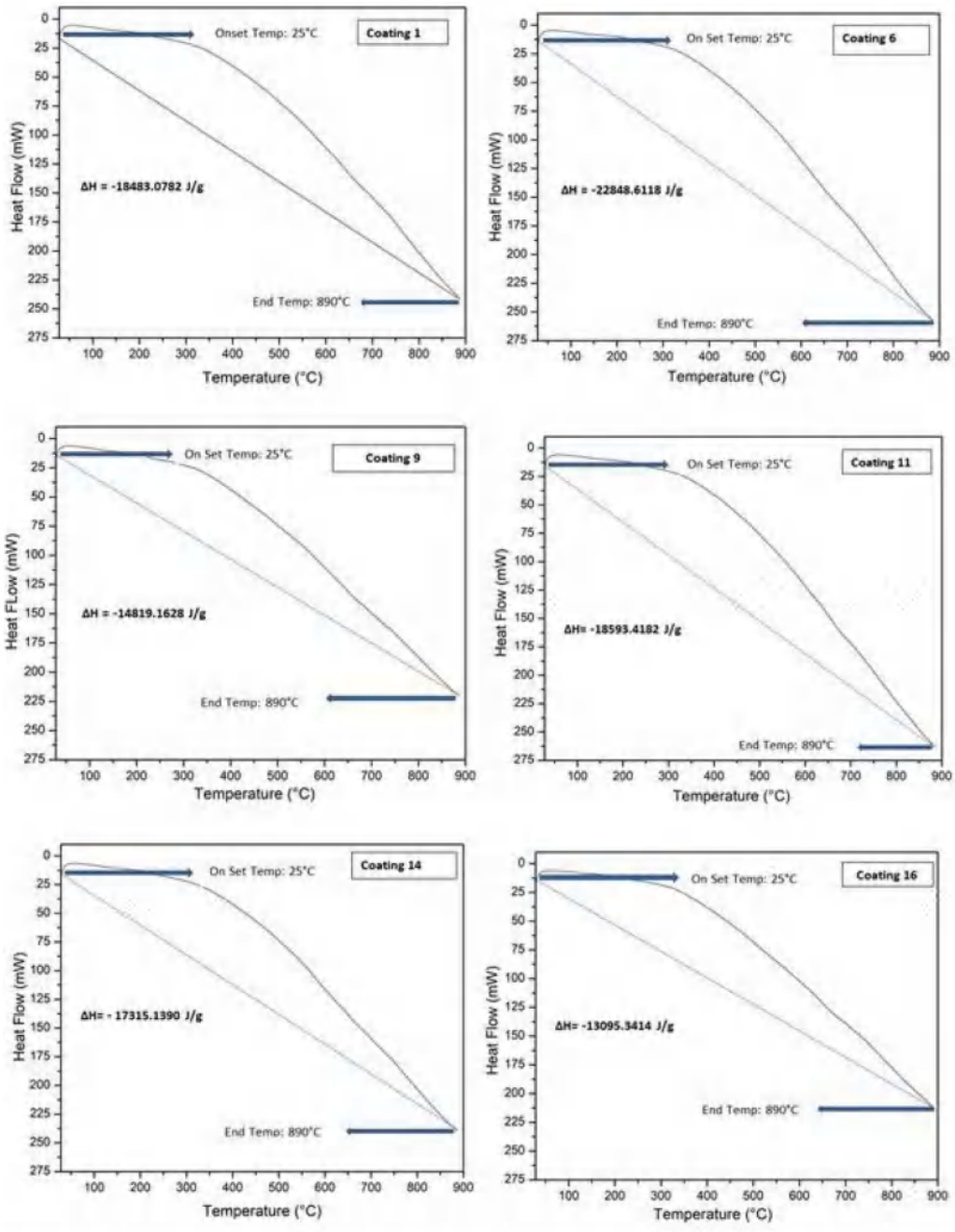

Fig. 6. Heat flow curve for coating mixture.

hence, the heat was released by the system. Here the process under consideration is exothermic in nature. The heat released during the heating of the electrode coating should not be very high as this may lead to an adverse impact on the weld region, heat affected zone leading up to thermo-mechanical affected zone. Table 7 represents the enthalpy value associated with each coating mixture specimen. Results indicate coating mixture 2 has the lowest enthalpy value of 11770.0279 J/g, whereas coating 3 has the maximum enthalpy of 26157.3258 J/g associated with it. Fig. 6 represents the plot between heat flow and temperature for several coating mixtures. Analysis of this curve using peak and area under the curve method is used to determine the enthalpy values.

Structural characterization of coating mixtures was done using X-Ray Diffraction XRD (Fig. 7) and Fourier Transformation Infrared Spectroscopy FTIR (Fig. 8). XRD of all the coating mixtures is almost the same because of the same constituent mixture present in them. The different peaks shown in Fig. 7 represent the phases present in the coating powder.

FTIR curve between transmittance and wave number is almost similar for all coating specimens. The similarity is mainly because constituent minerals in all the coatings are the same. Available literature helps to identify the nature and type of different bonds present [27–30].

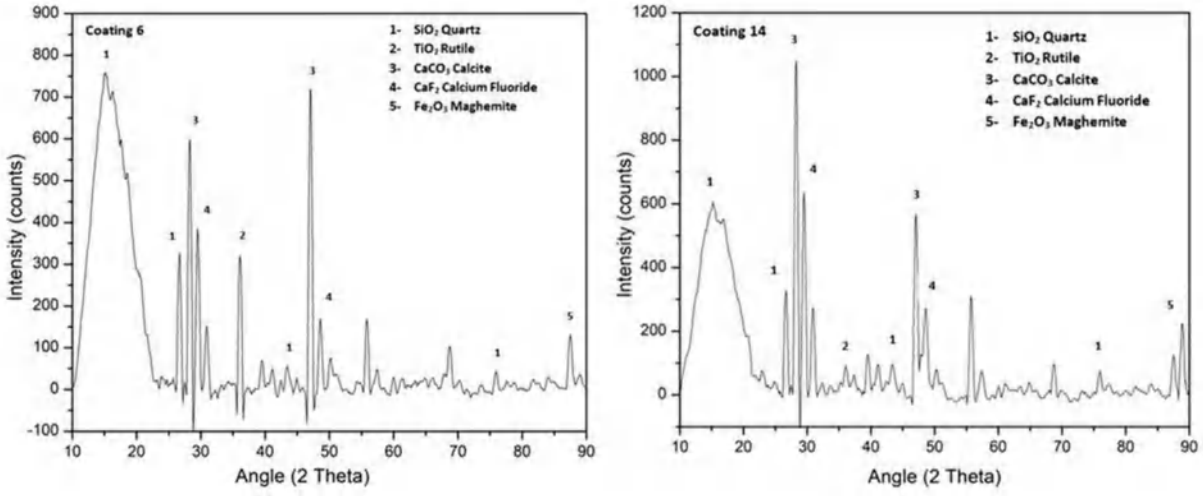

Fig. 7. XRD of electrode coatings.

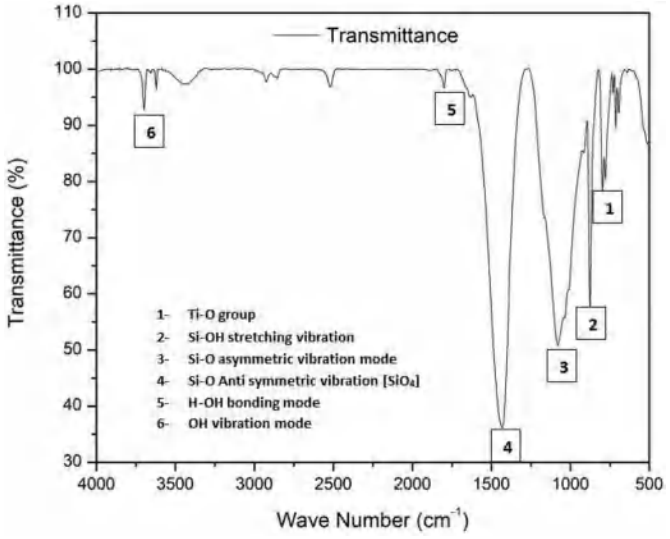

Fig. 8. FTIR curves of coating mixture.

A peak in the region of 700–750 cm^{-1} corresponds to symmetric stretching of the titanyl group (Ti–O), whereas one in the range 750–800 cm^{-1} represents Si–OH stretching vibrations. A peak in 1000–1250 cm^{-1} corresponds to Si–O asymmetric vibration mode. Anti-symmetric vibration of Si–O due to the formation of complex silicate ion [SiO_4^{4-}] is shown by peak lying in the 1250–1500 cm^{-1} range. Small peaks in the region of 1500–1750 cm^{-1} and 3250–3500 cm^{-1} represent H–OH bonding and OH vibration mode, respectively.

6. Development and discussion of regression model

Least square regression models for coating properties has been developed using statistical software package. Design Expert. The effect of minerals and their interactions on the electrode coating properties has been studied. Error percentage calculation gives us an estimate that how close the actual result is to the predicted result based on the developed model. Equations (9)–(14) below represents the regression models:

$$\text{Density (D)} = -0.45323\,CaO - 0.30242\,CaF_2 + 7.90995\times10^{-3}\,TiO_2 - 0.011693\,SiO_2 + 0.023061\,CaO{\cdot}CaF_2 + 0.012321\,CaO{\cdot}TiO_2 + 0.030548\,CaO{\cdot}SiO_2 + 3.66047\times10^{-3}\,CaF_2{\cdot}TiO_2 + 6.26017\times10^{-3}\,CaF_2{\cdot}SiO_2 - 0.026395\,TiO_2{\cdot}SiO_2 - 4.28377\times10^{-4}\,CaO{\cdot}CaF_2{\cdot}TiO_2 - 1.2139\times10^{-3}\,CaO{\cdot}CaF_2{\cdot}SiO_2 - 7.84805\times10^{-5}\,CaO{\cdot}TiO_2{\cdot}SiO_2 + 1.16853\times10^{-3}\,CaF_2{\cdot}TiO2{\cdot}SiO2 \quad (9)$$

$$\text{Thermal Diffusivity (TD)} = -0.075722\,CaO + 0.58821\,CaF_2 + 0.29142\,TiO_2 - 2.88523\,SiO_2 - 0.015329\,CaO{\cdot}CaF_2 - 7.20227\times10^{-3}\,CaO{\cdot}TiO_2 + 0.089024\,CaO{\cdot}SiO_2 - 0.033612\,CaF_2{\cdot}TiO_2 + 0.042418\,CaF_2{\cdot}SiO_2 + 0.057494\,TiO_2{\cdot}SiO_2 + 9.76046\times10^{-4}\,CaO{\cdot}CaF_2{\cdot}TiO_2 - 1.4204\times10^{-3}\,CaO{\cdot}CaF_2{\cdot}SiO_2 - 1.77628\times10^{-3}\,Cao.TiO_2{\cdot}SiO_2 + 2.03225\times10^{-4}\,CaF_2{\cdot}TiO_2{\cdot}SiO_2 \quad (10)$$

$$\text{Enthalpy (E)} = -9521.9998\,CaO - 1.49621\times10^{5}\,CaF_2 - 1.56028\,TiO_2 - 2.04702\,SiO_2 + 5898.45582\,CaO{\cdot}CaF_2 + 5881.32119\,CaO{\cdot}TiO_2 + 0.22212\,CaO.\,SiO_2 + 8551.42489\,CaF_2{\cdot}TiO_2 + 10177.64001\,CaF_2{\cdot}SiO_2 - 227.63392\,CaO{\cdot}CaF_2{\cdot}TiO_2 - 206.72584\,CaF_2{\cdot}TiO_2{\cdot}SiO_2 + 39.08316\,CaO{\cdot}SiO_2\,(CaO{-}SiO_2) - 118.79306\,CaF_2{\cdot}SIO_2\,(CaF_2{-}SiO_2) \quad (11)$$

$$\text{Specific Heat (SH)} = 1.15957\,CaO + 1.45556\,CaF_2 + 1.69540\,TiO_2 + 5.04638\,SiO_2 - 0.052764\,CaO{\cdot}CaF_2 - 0.061713\,CaO{\cdot}TiO_2 - 0.13434\,CaO{\cdot}SiO_2 - 0.068162\,CaF_2{\cdot}TiO_2 - 0.099968\,CaF_2{\cdot}SiO_2 - 0.16404\,TiO_2{\cdot}SiO_2 + 1.34202\times10^{-3}\,CaO{\cdot}CaF_2{\cdot}TiO_2 + 1.37168\times10^{-3}\,CaO{\cdot}CaF_2{\cdot}SiO_2 + 3.32928\times10^{-3}\,CaO{\cdot}TiO_2{\cdot}SiO_2 + 1.84925\times10^{-5}\,CaF_2{\cdot}TiO_2{\cdot}SiO_2 \quad (12)$$

$$\text{Weight Loss } (\Delta W) = -16.65314\,CaO - 15.27025\,CaF_2 - 19.551\,TiO_2 + 121.76639\,SiO_2 + 1.04742\,CaO{\cdot}CaF_2 + 1.08929\,CaO{\cdot}TiO_2 - 2.11269\,CaO{\cdot}SiO_2 + 1.21176\,CaF2{\cdot}TiO_2 - 3.8628\,CaF2{\cdot}SiO_2 - 2.54676\,TiO_2{\cdot}SiO_2 - 0.053509\,CaO{\cdot}CaF_2{\cdot}TiO_2 + 0.056358\,CaO{\cdot}CaF_2{\cdot}SiO_2 + 0.027196\,CaO{\cdot}TiO_2{\cdot}SiO_2 + 0.067243\,CaF_2{\cdot}TiO_2{\cdot}SiO_2 \quad (13)$$

$$\text{Thermal Conductivity (TC)} = 0.24251\,CaO + 0.91207\,CaF_2 + 0.80424\,TiO_2 - 1.39687\,SiO_2 - 0.027655\,CaO{\cdot}CaF_2 - 0.025563\,CaO{\cdot}TiO_2 + 0.049441\,CaO{\cdot}SiO_2 - 0.051677\,CaF2{\cdot}TiO_2 + 0.019250\,CaF2{\cdot}SiO_2 + 4.59608\times10^{-3}\,TiO_2{\cdot}SiO_2 + 1.3182\times10^{-3}\,CaO{\cdot}CaF_2{\cdot}TiO_2 - 1.1868\times10^{-3}\,CaO{\cdot}CaF_2{\cdot}SiO_2 - 6.52596\times10^{-4}\,CaO{\cdot}TiO_2{\cdot}SiO_2 + 7.34283\times10^{-4}\,CaF_2{\cdot}TiO_2{\cdot}SiO_2 \quad (14)$$

Table 8
ANOVA analysis.

Response	Source	Sum of Squares	df	Mean Square	F Values	P Values	Significance	R^2
Density	Model	0.010	13	7.85×10^{-4}	4.73	0.0221	Significant	0.74
	Linear Mixture	4.54×10^{-3}	3	1.51×10^{-3}	3.54	0.0375		
	$CaO{\cdot}CaF_2$	1.63×10^{-3}	1	1.63×10^{-3}	0.70	0.4302		
	$CaO{\cdot}TiO_2$	3.00×10^{-4}	1	3.00×10^{-4}	0.13	0.7304		
	$CaO{\cdot}SiO_2$	5.91×10^{-4}	1	5.91×10^{-4}	5.13	0.0176		
	$CaF_2{\cdot}TiO_2$	5.45×10^{-5}	1	5.45×10^{-5}	0.023	0.8828		
	$CaF_2{\cdot}SiO_2$	1.74×10^{-4}	1	1.74×10^{-4}	0.075	0.7923		
	$TiO_2{\cdot}SiO_2$	6.40×10^{-7}	1	6.40×10^{-7}	4.26	0.0293		
	$CaO{\cdot}CaF_2{\cdot}TiO_2$	1.84×10^{-4}	1	1.84×10^{-4}	0.079	0.7868		
	$CaO{\cdot}CaF_2{\cdot}SiO_2$	1.87×10^{-3}	1	1.87×10^{-3}	0.80	0.3999		
	$CaO{\cdot}TiO_2{\cdot}SiO_2$	7.83×10^{-6}	1	7.83×10^{-6}	3.3×10^{-3}	0.9554		
	$CaF_2{\cdot}TiO_2{\cdot}SiO_2$	1.73×10^{-3}	1	1.73×10^{-3}	0.74	0.4168		
	Residual	0.016	7	2.33×10^{-3}				
	Cor Total	0.027	20					
Weight Loss	Model	30.43	13	2.34	7.32	0.0154	Significant	0.77
	Linear Mixture	15.35	3	5.12	1.05	0.4284		
	$CaO{\cdot}CaF_2$	0.014	1	0.014	2.9×10^{-3}	0.9581		
	$CaO{\cdot}TiO_2$	0.24	1	0.24	6.08	0.0251		
	$CaO{\cdot}SiO_2$	1.60	1	1.60	5.27	0.0337		
	$CaF_2{\cdot}TiO_2$	0.057	1	0.057	0.012	0.9169		
	$CaF_2{\cdot}SiO_2$	2.06	1	2.06	0.42	0.5366		
	$TiO_2{\cdot}SiO_2$	0.95	1	0.95	4.65	0.0412		
	$CaO{\cdot}CaF_2{\cdot}TiO_2$	2.88	1	2.88	0.59	0.4675		
	$CaO{\cdot}CaF_2{\cdot}SiO_2$	4.04	1	4.04	0.83	0.3928		
	$CaO{\cdot}TiO_2{\cdot}SiO_2$	0.94	1	0.94	6.38	0.0225		
	$CaF_2{\cdot}TiO_2{\cdot}SiO_2$	5.75	1	5.75	1.18	0.3132		
	Residual	34.12	7	4.87				
	Cor Total	64.55	20					
Enthalpy	Model	2.79×10^8	13	2.62×10^7	7.47	0.0064	Significant	0.93
	Linear Mixture	2.62×10^7	3	8.73×10^6	3.03	0.1026		
	$CaO{\cdot}CaF_2$	8.79×10^6	1	8.79×10^6	3.05	0.1241		
	$CaO{\cdot}TiO_2$	2.16×10^7	1	2.16×10^7	7.52	0.0289		
	$CaO{\cdot}SiO_2$	1.17×10^5	1	1.17×10^5	0.041	0.8459		
	$CaF_2{\cdot}TiO_2$	3.83×10^7	1	3.83×10^7	13.31	0.0082		
	$CaF_2{\cdot}SiO_2$	253.43	1	253.43	8.79×10^5	0.9928		
	$TiO_2{\cdot}SiO_2$	7.99×10^6	1	7.99×10^6	2.78	0.1396		
	$CaO{\cdot}CaF_2{\cdot}TiO_2$	5.22×10^7	1	5.22×10^7	18.13	0.0038		
	$CaO{\cdot}CaF_2{\cdot}SiO_2$	4.59×10^7	1	4.59×10^7	15.97	0.0052		
	$CaO{\cdot}TiO_2{\cdot}SiO_2$	9.37×10^6	1	9.37×10^6	3.25	0.1143		
	$CaF_2{\cdot}TiO_2{\cdot}SiO_2$	7.34×10^7	1	7.34×10^7	25.50	0.0015		
	Residual	2.01×10^7	7	2.88×10^6				
	Cor Total	3.00×10^8	20					
Thermal Conductivity	Model	0.011	13	8.22×10^{-4}	7.3	0.04716	Significant	0.82
	Linear Mixture	4.005×10^{-3}	3	1.33×10^{-3}	1.45	0.3086		
	$CaO{\cdot}CaF_2$	2.312×10^{-7}	1	2.312×10^{-7}	2.5×10^{-4}	0.9878		
	$CaO{\cdot}TiO_2$	3.291×10^{-4}	1	3.291×10^{-4}	0.36	0.5691		
	$CaO{\cdot}SiO_2$	4.76×10^{-6}	1	4.76×10^{-6}	8.1	0.0321		
	$CaF_2{\cdot}TiO_2$	1.42×10^{-3}	1	1.42×10^{-3}	1.55	0.2535		
	$CaF_2{\cdot}SiO_2$	8.54×10^{-6}	1	8.54×10^{-6}	9.2×10^{-3}	0.9260		
	$TiO_2{\cdot}SiO_2$	1.60×10^{-6}	1	1.60×10^{-6}	6.9	0.0387		
	$CaO{\cdot}CaF_2{\cdot}TiO_2$	1.74×10^{-3}	1	1.74×10^{-3}	1.89	0.2113		
	$CaO{\cdot}CaF_2{\cdot}SiO_2$	1.79×10^{-3}	1	1.79×10^{-3}	1.94	0.2060		
	$CaO{\cdot}TiO_2{\cdot}SiO_2$	5.42×10^{-4}	1	5.42×10^{-4}	8.72	0.02527		
	$CaF_2{\cdot}TiO_2{\cdot}SiO_2$	6.86×10^{-4}	1	6.86×10^{-4}	0.74	0.4170		
	Residual	6.45×10^{-3}	7	9.22×10^{-4}				
	Cor Total	0.017	20					
Thermal Diffusivity	Model	0.015	13	1.18×10^{-3}	5.1	0.0418	Significant	0.78
	Linear Mixture	1.25×10^{-3}	3	4.18×10^{-4}	0.18	0.9050		
	$CaO{\cdot}CaF_2$	2.78×10^{-5}	1	2.78×10^{-5}	0.012	0.9154		
	$CaO{\cdot}TiO_2$	1.39×10^{-4}	1	1.39×10^{-4}	0.061	0.8123		
	$CaO{\cdot}SiO_2$	6.48×10^{-6}	1	6.48×10^{-6}	2.82×10^{-3}	0.9591		
	$CaF_2{\cdot}TiO_2$	2.92×10^{-3}	1	2.92×10^{-3}	1.28	0.2960		
	$CaF_2{\cdot}SiO_2$	1.83×10^{-4}	1	1.83×10^{-4}	0.080	0.7857		
	$TiO_2{\cdot}SiO_2$	2.08×10^{-5}	1	2.08×10^{-5}	9.09×10^{-3}	0.9267		
	$CaO{\cdot}CaF_2{\cdot}TiO_2$	9.57×10^{-4}	1	9.57×10^{-4}	0.42	0.5391		
	$CaO{\cdot}CaF_2{\cdot}SiO_2$	2.56×10^{-3}	1	2.56×10^{-3}	1.12	0.3255		
	$CaO{\cdot}TiO_2{\cdot}SiO_2$	4.01×10^{-3}	1	4.01×10^{-3}	7.15	0.0227		
	$CaF_2{\cdot}TiO_2{\cdot}SiO_2$	5.25×10^{-5}	1	5.25×10^{-5}	0.023	0.8840		
	Residual	0.016	11	2.29×10^{-3}				
	Cor. Total	0.031	20					

(*continued on next page*)

Table 8 (*continued*)

Response	Source	Sum of Squares	df	Mean Square	F Values	P Values	Significance	R^2
Specific Heat	Model	0.10	13	7.8×10^{-3}	4.73	0.02913	Significant	0.71
	Linear Mixture	0.044	3	0.015	1.46	0.3065		
	$CaO{\cdot}CaF_2$	6.472×10^{-4}	1	6.47×10^{-4}	0.064	0.8072		
	$CaO{\cdot}TiO_2$	0.012	1	0.012	1.15	0.3196		
	$CaO{\cdot}SiO_2$	3.87×10^{-6}	1	3.87×10^{-6}	3.84	0.03761		
	$CaF_2{\cdot}TiO_2$	3.2×10^{-3}	1	3.2×10^{-3}	0.32	0.5906		
	$CaF_2{\cdot}SiO_2$	1.57×10^{-3}	1	1.57×10^{-3}	0.16	0.7041		
	$TiO_2{\cdot}SiO_2$	2.11×10^{-4}	1	2.11×10^{-4}	0.021	0.8889		
	$CaO{\cdot}CaF_2{\cdot}TiO_2$	1.81×10^{-3}	1	1.81×10^{-3}	0.18	0.6844		
	$CaO{\cdot}CaF_2{\cdot}SiO_2$	2.39×10^{-3}	1	2.39×10^{-3}	5.79	0.01793		
	$CaO{\cdot}TiO_2{\cdot}SiO_2$	0.014	1	0.014	1.40	0.2753		
	$CaF_2{\cdot}TiO_2{\cdot}SiO_2$	4.35×10^{-3}	1	4.35×10^{-3}	0.43	0.5320		
	Residual	0.071	11	0.010				
	Cor. Total	0.17	20					

Table 9
Effect of mixture components on weld chemistry and hardness.

Nature	Term	Density (D)	Weight Loss (ΔW)	Enthalpy (ΔH)	Conductivity (TC)	Diffusivity (TD)	Specific Heat (SH)
Individual	Cao	+	–	–	–	–	–
	CaF_2	+	–	–	–	–	–
	TiO_2	+	–	–	–	–	–
	SiO_2	+	–	–	–	–	–
Binary	$CaO{\cdot}CaF_2$	–	–	–	–	–	–
	$CaO{\cdot}TiO_2$	–	+	+	–	–	–
	$CaO{\cdot}SiO_2$	+	+	–	+	–	+
	$CaF_2{\cdot}TiO_2$	–	–	+	–	–	–
	$CaF_2{\cdot}SiO_2$	–	–	–	–	–	–
	$TiO_2{\cdot}SiO_2$	+	+	–	+	–	–
	$CaO{\cdot}SiO_2(CaO–SiO_2)$			–			
	$CaF_2{\cdot}SiO_2(CaF_2–SiO_2)$			+			
Tertiary	$CaO{\cdot}CaF_2{\cdot}TiO_2$	–	–		–	–	–
	$CaO{\cdot}CaF_2{\cdot}SiO_2$	–	–		–	–	+
	$CaO{\cdot}TiO_2{\cdot}SiO_2$	–	+		+	+	–
	$CaF_2{\cdot}TiO_2{\cdot}SiO_2$	–	–		–	–	–

[+: Synergism; -: Anti Synergism].

The above-developed models were subjected to F Test using analysis of variance for adequacy. Independent analysis of these models has been done using linear, quadratic, special cubic and cubic models with backward and forward interpolations. The acceptance value P is kept at 95%. Table 8 represents the ANOVA analysis of each developed model.

The ANOVA analysis also helped us to ascertain the influence of individual components and their binary, tertiary interaction on the responses. The influences are categorized as synergistic (+) and anti-synergistic (−) based on their positive and negative impact on the response. The individual components and interactions having p-value less than 0.05 contribute synergistically, whereas the ones with p-value greater than 0.05 are anti-synergic. Table 9 represents the effect of mixture components on weld metal chemistry, and micro-hardness.

A plot between actual and predicted value for each response helps us to ascertain the closeness of values obtained from the predicted equation to the line of best fit. Fig. 9(a–f) presents the same.

Analysis of the regression model indicates that coating constituents affect the thermal and physicochemical properties of electrode coating significantly. The electrode coating is exposed to high-temperature ranges during the welding process. Exposure to high temperatures causes several chemical reactions to occur. Sound performance in such an environment requires high thermal stability, minimum weight loss, and suitable enthalpy of the fusion reaction, increased thermal conductivity, suitable diffusivity, and specific heat. Individual behavior of coating mineral constituents, along with their interaction with each other, determines their performance characteristics. Coating mixture melts and gets dissolved into the molten weld pool with base metal and filler wire. The density of the coating mixture should be good to ensure the restricted fluidity of the weld pool. A highly fluid weld pool will leads spreading before solidification and can give rise to several defects. SiO_2 is known as network/chain former, which decreases fluidity and increases the density of the pool. CaO and SiO_2 together form $SiO_4{}^{4-}$ complex silicate ion by the following chemical reaction: $CaO = Ca^{2+} + O^{2-}$; $SiO_2 + 2O^{2-} = SiO_4{}^{4-}$. This silicate ion makes the diffusion of inclusions difficult and hence increases density. As per the regression model, individual constituents and SiO_2 containing binary interaction such as $TiO_2{\cdot}SiO_2$, $CaO{\cdot}SiO_2$ has a synergistic effect on the density of the coating, whereas other binary and tertiary interactions are anti-

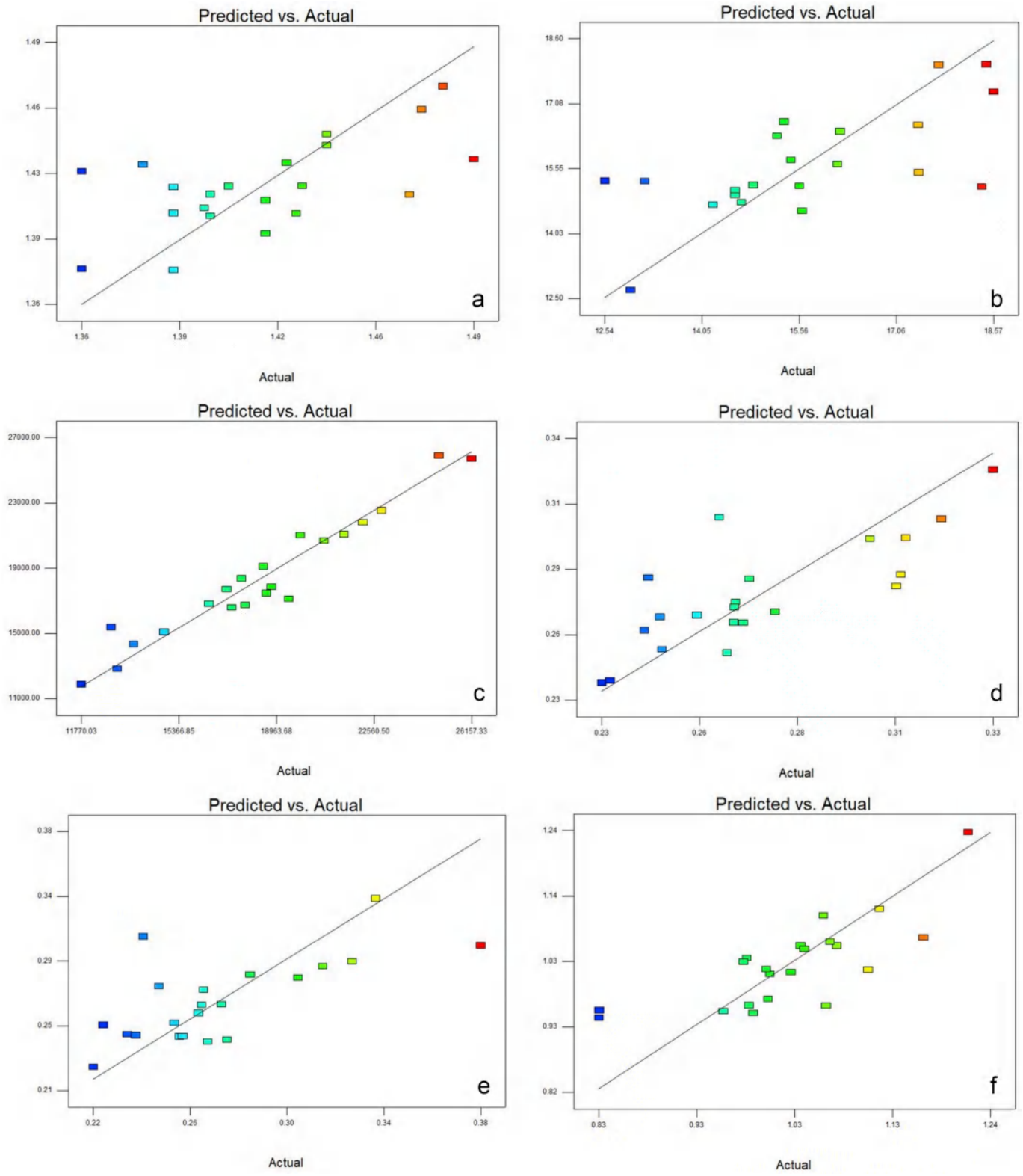

Fig. 9. Predicted versus Actual plot of: (a) Density (b) Weight Loss (c) Enthalpy (d) Thermal Conductivity (e) Thermal Diffusivity (f) Specific Heat.

synergistic to density. The developed cubic regression model has a p-value of 0.0221, which is under the acceptable confidence level of 95%. The coating is expected to be thermally stable at high temperatures. Thermal stability in this work has been measured using Thermogravimetric Analyzer, where weight loss has been calculated by heating in a controlled environment. The melting point of calcite (CaO) is around 2572 ˚C, fluorspar (CaF_2) is 1418 ˚C, rutile (TiO_2) is 1843 ˚C, and for silica (SiO_2) it is around 1710 ˚C. As per the regression model analysis for weight loss, it is evident that binary interactions $CaO{\cdot}TiO_2$, $CaO{\cdot}SiO_2$, $TiO_2{\cdot}SiO_2$ and tertiary interaction $CaO{\cdot}TiO_2{\cdot}SiO_2$ tend to

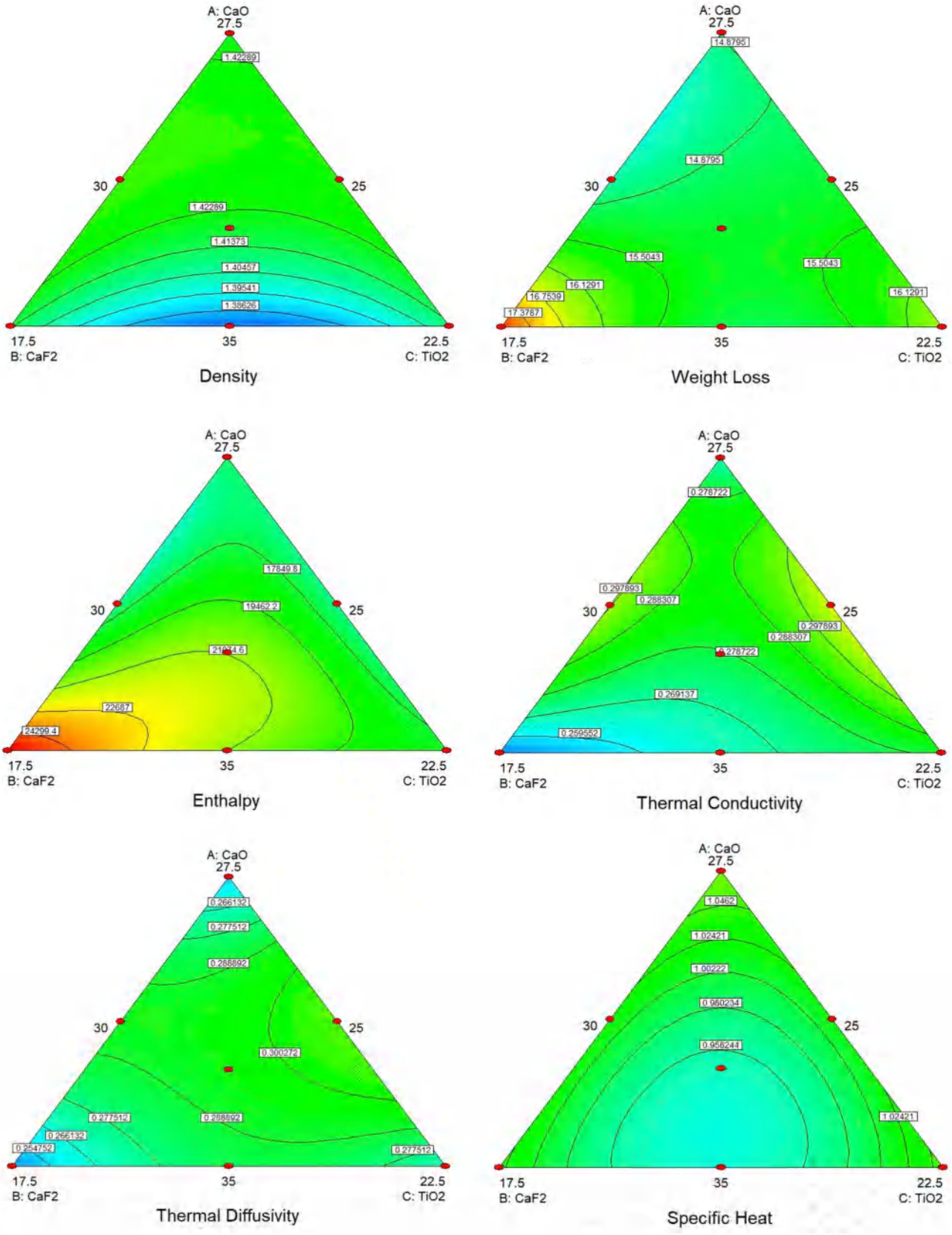

Fig. 10. Contour plots of measured properties.

Table 10
Target for response optimization.

Response	Target
Density	In Range
Weight Loss	Minimum
Enthalpy	In Range
Thermal Conductivity	Maximum
Thermal Diffusivity	In Range
Specific Heat	In Range

increase the thermal stability of coating, whereas all other interaction affects the property negatively. This model stands significant with a p-value of 0.0154. Enthalpy is the amount of energy in the form of heat, released or absorbed during chemical reactions. In this experiment, all enthalpy values came out to be negative, suggesting the reaction to be exothermic. The enthalpy value should neither be too high nor too low. A very high negative value of enthalpy implies a large amount of heat will be released during the welding process. It is not desirable as high heat produced will affect the base metal and will lead to increased heat affected zone area and other defects. The regression model of enthalpy is significant, with a p value of 0.0064. Binary interactions $CaO{\cdot}TiO_2$, $CaF_2{\cdot}TiO_2$ and tertiary interactions $CaO{\cdot}CaF_2{\cdot}TiO_2$, $CaF_2{\cdot}TiO_2{\cdot}SiO_2$ are synergistic to enthalpy, whereas all individual constituents and tertiary interactions are anti-synergistic. Synergistic interactions indicate that CaF_2 and TiO_2 are quite instrumental in increasing enthalpy value. Thermal properties of conductivity, diffusivity, and specific heat are also significantly dependent on coating composition. The regression model shows the dependency of thermal conductivity on synergistic binary interactions of $CaO{\cdot}SiO_2$, $TiO_2{\cdot}SiO_2$ and tertiary interaction of $CaO{\cdot}TiO_2{\cdot}SiO_2$, with a p-value of model being 0.0064. Similarly, thermal diffusivity has a significant regression model with p-value, 0.0418 and its synergistic factor is tertiary interaction of calcite, rutile, and silica. Specific heat is the amount of heat required to produce a unit increase in temperature of a unit mass of coating mixture. Specific heat should not be very high as it will require lots of energy to provide melting and fusion heat to the electrode. On the other hand, low specific heat will cause the temperature to increase from a very low heat input and will correspondingly cause very high temperature during the process. This will eventually lead to the release of a huge amount of heat in an exothermic process and will affect the weld adversely. As per the regression model with p-value of 0.02913, the synergistic factors for specific heat are binary interactions $CaO{\cdot}SiO_2$ and tertiary interaction $CaO{\cdot}CaF_2{\cdot}SiO_2$.

7. Contour Plots

Contour plots are the representation of the variation of response value over the changing value of input parameters. The different colors of contour show the different range of values of a particular response that can be achieved. Moreover, the lines running across the plot represent the constant value of output response with the variation in mixture composition. Fig. 10 represents the contour plot for various measured properties.

8. Multi response optimization

The actual responses were optimized using multi response technique. Table 10 presents the target for each response which was used to obtain optimum solution.

Using the above response-target combination the following optimum solution was achieved (Table 11).

The achieved solutions have a desirability of 69.1%, 68.9%, 68.7%, 67.2% and 61.1% respectively. Fig. 11 shows the contour plot of optimum solutions obtained.

9. Model validation

The developed regression model has been validated using four compositions chosen at random from the design matrix. The predicted value obtained from the models is compared with the actual value obtained from the experiment. This is done to estimate the concurrency of the regression model with the actual results. Table 12 presents validation for density, weight loss, and enthalpy, whereas Table 13 presents the same for conductivity, diffusivity, and specific heat.

10. Conclusions

- Calcite, fluorspar, rutile, silica, and iron ore mineral waste red ochre were mixed in different proportions based on extreme vertices design to obtain twenty-one electrode coating formulation.
- The coatings were examined for various physico-chemical and thermal properties, which include: density, weight loss as a measure of thermal stability, enthalpy change, thermal conductivity, thermal diffusivity, and specific heat.
- Structural analysis of powders has been done using X-Ray Diffraction (XRD) and Fourier Transformation Infrared spectroscopy (FTIR)
- A regression model of each property was developed, and its significance was checked by keeping an acceptable confidence level of 95%.
- An attempt has been made to analyze the effect of an individual component, their binary and tertiary interaction on each property.
- Individual mineral constituents and SiO_2 containing binary interaction such as $TiO_2.SiO_2$, $CaO.SiO_2$ affects density synergistically. CaO and SiO_2 react chemically to form complex silicate ion [SiO_4^{4-}]. Silicate ion plays an influential role in increasing the density of the electrode coating.
- For weight loss as a measure of thermal stability, it is clearly evident that binary interactions $CaO{\cdot}TiO_2$, $CaO{\cdot}SiO_2$, $TiO_2{\cdot}SiO_2$ and tertiary interaction $CaO{\cdot}TiO_2{\cdot}SiO_2$ tends to increase the thermal stability of the coating.
- Binary interactions $CaO{\cdot}TiO_2$, $CaF_2{\cdot}TiO_2$ and tertiary interactions $CaO{\cdot}CaF_2{\cdot}TiO_2$, $CaF_2{\cdot}TiO_2{\cdot}SiO_2$ are synergistic to enthalpy whereas all individual constituents and tertiary interactions are anti-synergistic.
- Thermal conductivity depends synergistically on binary interactions of $CaO{\cdot}SiO_2$, $TiO_2{\cdot}SiO_2$ and tertiary interaction of $CaO{\cdot}TiO_2{\cdot}SiO_2$.
- Thermal diffusivity has a significant regression model with p-value 0.0418 and its synergistic factor is tertiary interaction of $CaO{\cdot}TiO_2{\cdot}SiO_2$.

Table 11
Optimum solution.

Sol.	Cao	CaF_2	TiO_2	SiO_2	ρ	ΔW	ΔH	TC	TD	SH	Desir.
1	29.13	25.00	26.36	9.49	1.45	14.49	17999.5	0.3046	0.2611	1.171	0.691
2	28.44	25.00	26.64	9.91	1.46	14.25	18908.2	0.3002	0.2438	1.211	0.689
3	27.97	25.00	27.02	10.00	1.46	14.07	19287.9	0.2973	0.2400	1.214	0.687
4	30.24	21.95	30.00	7.80	1.43	14.25	16468.8	0.2971	0.2884	1.027	0.672
5	35.00	22.20	22.79	10.00	1.42	16.09	16162.7	0.3252	0.3214	1.016	0.611

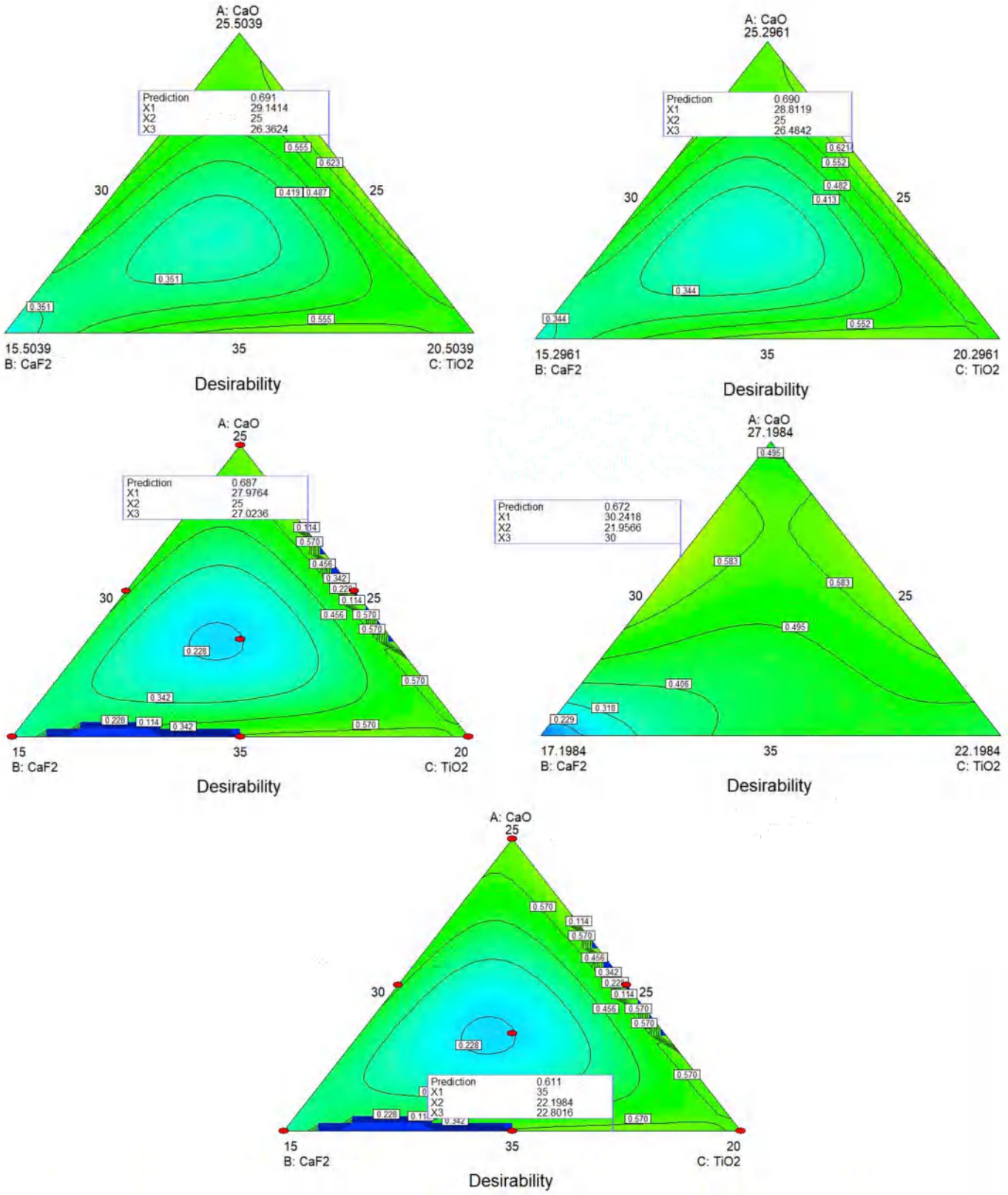

Fig. 11. Contour Plots of desirability.

- Synergistic factors for specific heat are binary interactions $CaO{\cdot}SiO_2$ and tertiary interaction $CaO{\cdot}CaF_2{\cdot}SiO_2$.
- The developed models have been optimized using multi-response optimization. Five optimum solutions were achieved and their desirability in % is 69.1, 68.9, 68.7, 67.2, and 61.1 respectively.
- Model validation has been done by finding error percentage between predicted and actual values of each property for four different mixture compositions chosen at random. The error percentage is well under limit and shows little deviation between actual and predicted values.

Table 12
Error (%) in chemical composition: Density, Weight Loss and Enthalpy.

Coating Mixture				Predicted Value			Actual Value			% Error		
CaO	CaF_2	TiO_2	SiO_2	ρ	ΔW	ΔH	ρ	ΔW	ΔH	ρ	ΔW	ΔH
30	25	25	10	1.456	14.76	19097.81	1.471	14.66	18483.12	1.019	0.682	3.32
35	25	25	5	1.418	16.56	15078.19	1.408	17.40	14819.16	0.705	4.82	1.74
35	20	30	5	1.405	17.97	16736.52	1.43	17.72	17811.37	1.78	1.45	6.03
30	20	30	10	1.405	14.69	14329.83	1.39	14.22	13693.78	0.714	3.3	4.64

Table 13
Error (%) in chemical composition: Conductivity, Diffusivity and Specific Heat.

Coating Mixture				Predicted Value			Actual Value			% Error		
CaO	CaF_2	TiO_2	SiO_2	TC	TD	SH	TC	TD	SH	TC	TD	SH
30	25	25	10	0.260	0.243	1.232	0.320	0.264	1.214	18.8	7.94	1.5
35	25	25	5	0.263	0.260	1.014	0.267	0.260	1.028	1.68	0.11	1.36
35	20	30	5	0.237	0.225	1.056	0.233	0.217	1.076	1.71	3.46	1.85
30	20	30	10	0.269	0.254	1.064	0.267	0.250	1.069	0.59	1.49	0.46

References

[1] B. Mvola, P. Kah, J. Marlikainen, R. Suoranta, Dissimilar welded joints operating in sub-zero temperature environment, Int. J. Adv. Manuf. Technol. 87 (2016) 3619–3635.
[2] E.J. Barnhouse, J.C. Lippold, Microstructure/Property relationships in dissimilar welds between duplex stainless steels and carbon steels, Weld. Res. (1998) 477s–488s.
[3] Jan Olsson, Malin Snis, Duplex- A new generation of stainless steel for desalination plants, Desalination 205 (2007) 104–113.
[4] M. Sadeghian, M. Shamanian, A. Shafyei, Effect of heat input on microstructure and mechanical properties on dissimilar joints between super duplex stainless steel and high strength low alloy steel, Mater. Des. 60 (2014) 678–684.
[5] Dinesh W. Rathod, Sunil Pandey, P.K. Singh, Rajesh Prasad, Experimental Analysis of dissimilar metal weld joint: ferritic to austenitic stainless steel, Mater. Sci. Eng. A 639 (2015) 259–268.
[6] R. Chhibber, N. Arora, S.R. Gupta, B.K. Dutta, Use of bimetallic welds in nuclear reactors: associated problems and structural integrity assessment issues, Proc. IMechE Part C: J. Mech. Eng. Sci. (220) (2016) 1121–1133.
[7] Brahmin Belkessa, Djamel Miroud, Naima Ouali, Billel Cheniti, Microstructure and mechanical behavior in dissimilar SAF 2205/API X52 welded pipes", Acta Metall. Sin. 29 (7) (2016) 674–682.
[8] Deepak Bhandari, Rahul Chhibber, Navneet Arora, Rajeev Mehta, Investigation on weld metal chemistry and mechanical behavior of bimetallic welds using CaO-CaF2-SiO2-Ni based electrode coatings, Proc. IMechE Part L: J Mater. Design Appl. 233 (4) (2019) 563–579.
[9] Deepak Bhandari, Rahul Chhibber, Navneet Arora, Rajeev Mehta, TiO2-SiO2-Cao-CaF2 based electrode coatings on weld metal chemistry and mechanical behavior of bimetallic welds, J. Manuf. Process. 23 (2016) 61–74.
[10] Lochan Sharma, Rahul Chhibber, Design TiO2-SiO2-MgO and SIO2-MgO-Al2O3 based submerged arc fluxes for multipass bead on plate pipeline steel welds, J. Press. Vessel Technol. 141 (2019) 041402-1-041402-12.
[11] Lochan Sharma, Rahul Chhibber, Design Cao-SiO2-CaF2 and Cao-SiO2-Al2O3 based submerged arc fluxes for series of beads on plate pipeline steel welds- Effect of Carbon and Manganese content, Grain size and micro hardness, J. Press. Vessel Technol. 141 (2019) 031403-1-031403-10.
[12] Sandeep Jindal, Rahul Chhibber, N.P. Mehta, Investigation on flux design for submerged arc welding of high strength low alloy steel, Proc. IMechE, Part B: J. Eng. Manuf. 227 (3) (2013) 383–395.
[13] Sumit Mahajan, Rahul Chhibber, Design and development of shielded Metal Arc welding (SMAW) electrode coating using a CaO-CaF2-SiO2 and CaO-SiO2-Al2O3 flux system, J. Occup. Med. 71 (7) (2019) 2435–2444.
[14] Lochan Sharma, Rahul Chhibber, Design and Development of submerged arc welding fluxes using TiO2-SiO2-CaO and SiO2-CaO-Al2O3 flux system, Proc. IMechE Part E: J. Process Mech. Eng. 233 (4) (2019) 739–762.
[15] Lochan Sharma, Rahul Chhibber, Investigating the physicochemical and thermo-physical properties of submerged arc welding fluxes designed using TiO2-SiO2-MgO and SiO2-MgO-Al2O3 flux systems for linepipe steels, Ceram. Int. 45 (2) (2018) 1569–1587 Part A.
[16] Daniel M. Franks, David V. Boger, Claire M. Cote, David R. Mulligan, Sustainable development principles for the disposal of mining and mineral processing wastes, Resour. Policy 36 (2011) 114–122.
[17] Yassine Taha, Mostafa Benzaazoua, Rachid Hakkou, Mohammed Mansori, Natural clay substitution by calamine processing wastes to manufacture fired bricks, J. Clean. Prod. 135 (2016) 847–858.
[18] Sapana Garu, Sudhir Sitaram Amritphale, Jyotishankar Mishra, Smita Joshi, Multicomponent red mud polyster composites for neutron shielding applications, Mater. Chem. Phys. 224 (2019) 369–375.
[19] S. Vigneshwaran, M. Uthayakumar, V. Arumugaprabu, Development and sustainability of industrial waste based red mud hybrid composites, J. Clean. Prod. 230 (2019) 862–868.
[20] Yuancheng Li, Xiaobo Min, Yong Ke, Degang Liu, Chongjian Tang, Preparation of red mud based geopolymer materials from MSWI fly ash and red mud by mechanical activation, Waste Manag. 83 (2019) 202–208.
[21] P. Ambroza, L. Kavaliauskiene, Utilisation of waste material for welding and surfacing, Mechanika 2 (70) (2008) 56–60.
[22] Emile Mukiza, LingLing Zhang, Xiaoming Liu, Na Zhang, Utilization of red mud in road base and subgrade materials: a Review, Resour. Conserv. Recycl. 141 (2019) 187–199.
[23] V.L. Anderson, R.A. McLean, Design of Experiments: a Realistic Approach, Marcell Dekker, New York, 1974.
[24] Sandeep Jindal, Rahul Chhibber, N.P. Mehta, Investigation on flux design for submerged arc welding of high strength low alloy steel, Proc. IMechE, Part B: J. Eng. Manuf. 227 (3) (2013) 383–395.
[25] After A. Muan, E.F. Obsorn, Phase Equilibria Among Oxides in Steel Making, Addison Wesley, Reading M.A, Fig, 1965, p. 82.
[26] Joydeb Mukherjee, Phase equilibrium diagram CaO-CaF2-2CaO.SiO2, J. Am. Ceram. Soc. 48 (4) (1965) 210–213.
[27] G. Kaur, M. Kumar, A. Arora, O.P. Pandey, K. Singh, Influence of Y_2O_3 on structural and optical properties of SiO_2-BaO-ZnO-xB_2O_3-(10-x) Y_2O_3 glasses and glass ceramics, J. Non-Cryst. Solids 357 (2011) 857–863.
[28] M. Garai, N. Sasmal, A.R. Molla, B. Karmakar, Structural effects of Zn + 2/Mg + 2 ratios on crystallization characteristics and microstructure of fluorophlogopite mica-containing glass ceramics, Solid State Sci. 44 (2015) 10–21.
[29] M. Garai, N. Sasmal, A.R. Molla, S.P. Singh, A. Tarafder, B. Karmakar, Effect of nucleating agents on crystallization and microstructure of fluorophlogopite mica-containing glass ceramics, J. Mater. Sci. 49 (4) (2014) 1612–1623.
[30] T.Sowmya, S.R.Sankaranarayanan, Spectroscopic analysis of slags-preliminary observations, VII International Conference on Molten Slags, Fluxes and Salts, The South African Institute of Mining and Metallurgy.